Heterotypic intercellular adhesion tunes efficiency of cell-on-cell migration

Chandrashekar Kuyyamudi[1,2]*#, Suhrid Ghosh[1,2]#, & Cassandra G. Extavour[1,2,3]*

1. Department of Organismic & Organismic Biology, Harvard University. Cambridge, MA, USA
2. Howard Hughes Medical Institute. Chevy Chase, MD, USA
3. Department of Molecular & Cellular Biology, Harvard University. Cambridge, MA, USA

* Correspondence: CK ckuyyamudiashwinikumar@fas.harvard.edu

CGE extavour@oeb.harvard.edu

# These authors contributed equally.

Abstract

Cell migration across epithelial barriers occurs in diverse developmental, immunological, and pathological contexts. Here we investigate the contribution of heterotypic adhesion between migrating cells and epithelial "substrate" cells to transepithelial migration. Using an *in silico* model inspired by the migration of primordial germ cells across the midgut epithelium in the *Drosophila* embryo, we show that heterotypic adhesion modulates migration efficiency in a non-monotonic manner, revealing the existence of an optimal adhesion regime. Consistent with this prediction, *in vivo* overexpression of E-cadherin in germ cells accelerated their exit from the midgut relative to controls. Beyond providing experimentally testable predictions, our model integrates and explains previous observations on the role of heterotypic adhesion in cell-on-cell migration, offering a framework for understanding transepithelial migration across biological contexts.

Keywords:

Germ cell migration, intercellular adhesion, E-cadherin, Cellular Potts model, CompuCell3D, *in vivo* live imaging

Introduction

Cells frequently carry out their functions at locations distinct from their site of origin, making the individual cellular motility that is required for cell migration a critical aspect of their behavior (1, 2). To achieve motility, cells require persistent and directed membrane activity, which is frequently guided by external chemical cues (3–6). This directed membrane activity is enabled by the dynamic nature of cell membranes, which exhibit continuous turnover of cytoskeletal components (7–9)

Cell migration, division, differentiation and death enable the development of multicellular organisms from a single cell (10). Cells in various developmental contexts migrate individually as well as collectively (1, 2, 11). Embryonic development unfolds as a tightly regulated cascade of events, where each step must occur within a specific time window to prevent disruption of subsequent stages (12–15). These temporal constraints also apply to cell migration, making not only the path taken but also the timing of arrival critical to proper development (1, 2, 16, 17).

In the developing embryo of the fruit fly *Drosophila melanogaster*, the primordial germ cells (germ cells) are the first cells to form (18). The germ cells form at the posterior tip of the embryo roughly 2.5 hours after egg laying (18, 19). Around 15 minutes after their formation, the embryo undergoes gastrulation, and the cluster of germ cells enters the primordial midgut upon invagination of the surrounding tissue during gastrulation (20). Here, the germ cell cluster eventually disassembles, and the germ cells exit the gut by individually passing through the monolayer of epithelial cells that form the midgut (20, 21). The proteins Wunen and Wunen2, which are expressed in the ventral midgut among other tissues, serve as repellents driving the germ cells to exit the midgut dorsally (22–25). Once outside the midgut, the germ cells continue their migration to join the mesodermal cells that form the somatic gonad primordium (26).

The *Drosophila* adhesion protein E-cadherin is encoded by the *shotgun* (*shg*) gene, and is maternally deposited in the early embryo (27, 28). Germ cells require this maternally deposited E-cadherin both to form a cohesive cluster and to tether to the invaginating midgut primordium during gastrulation (29–31). Regulation of germ cell E-cadherin during internalization into the midgut is orchestrated by the Trapped in endoderm (Tre1) protein, a G protein-coupled receptor (30, 31). Tre1 enables the germ

63 cell cluster to form a radial configuration of polarized cells that detach from the cluster
64 prior to transepithelial migration (30, 31). In embryos laid by females expressing a loss
65 of function *shotgun* allele (shg^{A9-49}), individual germ cells separate from the cluster
66 prematurely (30). Furthermore, in 38% of shg^{A9-49} mutant embryos, germ cells exhibit a
67 delay in crossing the midgut epithelium (30). The posterior midgut, which is the barrier
68 that the germ cells must breach, is made up of epithelial cells (32, 33). Remodeling of the
69 midgut epithelium endows the epithelial barrier with increased permeability, allowing
70 the germ cells to migrate through it (20, 34). High resolution imaging of the germ cells
71 crossing the midgut epithelium has shown that germ cells maintain contacts with the
72 epithelial cells with no evident intercellular space around them (20). In addition, FGF
73 signaling regulates the distribution of zygotic E-cadherin in the posterior midgut to
74 maintain its epithelial integrity (35). FGF mutants display mislocalized E-cadherin and
75 collapse of the midgut lumen, trapping the germ cells within (35).

76 Germ cells expressing defective E-cadherin (shg^{A9-49}) show delayed
77 transepithelial migration (30), reminiscent of the delay in border cell migration that
78 occurs when nurse cells either lack or overexpress E-cadherin in the *D. melanogaster* egg
79 chamber (36). Together, these observations suggest the existence of a non-monotonic
80 relationship between migration efficiency and adhesion between migrating and
81 substrate cells. We set out to understand the role of heterotypic adhesion between the
82 migrating cells and "substrate" cells in transepithelial migration, taking as a case study
83 the role of intercellular adhesion mediated by E-cadherin in enabling the germ cells to
84 transmigrate. Leveraging genetic tools and two-photon microscopy, we live imaged the
85 process of transepithelial migration *in vivo*. We combined the insights gained from live
86 imaging with previously published observations to formulate an *in silico* model of the
87 process. This model, formulated in the Cellular Potts Model framework (37–39),
88 provides a novel mechanistic understanding of this transepithelial migration process.
89 Our model reveals the existence of optimal heterotypic adhesion between germ cells
90 and the epithelial cells, which maximizes the efficiency of midgut exit. In addition, our
91 *in silico* model yields testable, potentially generalizable predictions about the role of E-
92 cadherin and intercellular adhesion that may be applicable to other systems of
93 heterotypic cell adhesion and migration.

Results

I. Germ cells exit the midgut individually and maintain E-cadherin expression throughout exit

To gain insight into the process of germ cell transepithelial migration, we live imaged the process *in vivo* [**Fig. 1b-b″**]. Before migration, the germ cells are contained by the epithelial barrier of the midgut [**Fig. 1b**], and located at a depth of more than 25μm from the cortex within the embryo (40). To visualize the germ cells, we used the previously generated fly line *nos-LifeAct-tdTomato* (41) which specifically labels germ cell membrane and cortex through posteriorly localized maternally deposited protein. The cells in the gut epithelium also show some residual labelling since the gut arises from the invaginating posterior blastoderm. The residual labelling generates contrast and helps us estimate the position of the gut during transepithelial migration.

We tracked germ cells throughout transepithelial migration, characterizing their progress at a five minute time resolution [**SI Videos 1 - 3**], and quantified the distances of germ cells from the center to the edge of the midgut lumen as a function of time [**Fig. 1 c**]. **Figure 1d-d′** shows the distance covered relative to their initial position (i.e. t = 0) as a function of time for two different embryos. We found that individual germ cells took 30 minutes on average to go through the midgut epithelial barrier [**Fig. 1d-d′; SI Videos 1 - 3**]. Our live imaging of the transepithelial migration process did not reveal any cell divisions in the midgut epithelial cells that could have generated spaces in the epithelial barrier that would allow for easier exit of germ cells, in contrast to the mechanism that regulates macrophage infiltration in *D. melanogaster* (42).

We also observed E-cadherin localization on the surface of germ cells during the transepithelial migration by immunostaining for GFP in endogenously GFP-tagged E-cadherin embryos [**Fig. 1e-e′**] , a result consistent with previously published experiments (30) that detected E-cadherin by immunostaining. We quantified the intensity of E-cadherin signal at apical and lateral junctions between midgut epithelial cells, as well as at the epithelial-germ cell junctions [**Fig 1e′′**]. Our quantification revealed that the E-cadherin concentration at the germ cell-epithelial cell interface is not significantly different from that observed between epithelial cells on the lateral side

124 [**Fig. 1e'**, p = 0.31]. The presence of E-cadherin in germ cells during transepithelial
125 migration, where germ cells physically contact epithelial cells (20), along with the
126 delayed midgut exit previously observed in *shg* loss of function mutants (30), suggests
127 that the expression of E-cadherin in germ cells is functional rather than incidental.

128

129 *II. Time to exit the midgut has a non-monotonic dependence on germ cell*
130 *E-cadherin level*

131 Although inspired by germ cell transepithelial migration, our central question is
132 broader: what role does heterotypic E-cadherin adhesion play in cell migration? To
133 generalize our question beyond germ cell transepithelial migration, we turned to *in*
134 *silico* modeling, retaining only essential features of the phenomenon. We developed a
135 two-dimensional model of transepithelial migration, where a single motile cell breaches
136 a ring of epithelial cells under the influence of an external, radial chemoattractant
137 gradient [**Fig. 2a**]. Our two-dimensional model, formulated as a Cellular Potts Model
138 (37, 38), enabled us to consider the cells as finite sized objects capable of deformations in
139 shape. We primarily explored the potential role of chemoattractant strength (λ_M) and
140 the concentration of E-cadherin in the germ cells (C_G) in the time taken for the germ cells
141 to exit the epithelial barrier (τ_e). We ran our simulations for a maximum of 10,000
142 Monte Carlo steps, and saved the position of the germ cell as a function of time for each
143 independent iteration for a given choice of system parameters. **Figure 2a** shows a
144 typical snapshot from our CompuCell3D simulation, and **Figure 2b-b''** shows the
145 modeled germ cell at three different stages of the transepithelial migration. In the CPM
146 framework, the temperature parameter (T) controls boundary pixel activity, where
147 higher temperatures increase the likelihood of energy-raising pixel flips. To investigate
148 how membrane fluctuations at interepithelial junctions affect migration, we modulated
149 the temperature governing pixel acceptance rates at these boundaries. This allowed us
150 to study how epithelial remodeling influences transepithelial migration.

151 Our simulations [**Fig. 2c-c′**] revealed that elevated epithelial temperature
152 increased tissue permeability to germ cells, resulting in faster exit times (τ_e) and higher
153 escape probabilities (p_e). This is consistent with prior experimental findings where
154 failure in epithelial remodeling of the midgut adversely affected germ cell
155 transepithelial migration (20, 34, 43).

156 The strength of the modeled chemoattractant λ_M beyond which germ cells
157 successfully migrated through the barrier was positively correlated with epithelial cell
158 E-cadherin concentration C_E [**Fig. 3a–a′′**]. We interpret this to mean that higher C_E
159 values, indicating stronger adhesion between the epithelial cells, offered greater
160 resistance to the trans-migrating cell. Regardless of the value of C_E, we observed that
161 the time taken to exit the barrier decreased with increased germ cell E-cadherin
162 concentration only up to a point, beyond which there was a sharp increase in the time
163 taken to breach the epithelial barrier [**Fig. 3a–a′′**]. This non-monotonic dependence of τ_e
164 on C_G suggested that there is an optimal range of heterotypic adhesion between germ
165 cell and the epithelial cell. Within this range, adhesion aids the transepithelial
166 migration, but beyond the range, it hinders germ cell movement. The minima of the
167 curves for different values of λ_M in **Figure 3a–a′′** coincide, indicating that the optimal
168 adhesion value for transepithelial migration is independent of the chemoattractant
169 strength. Interestingly, the coefficient of variation in the time to exit τ_e as a function of
170 C_G has a trend that is inverse of the one exhibited by τ_e [**Fig. 3b**]. Specifically, the
171 coefficient of variation is highest when the mean is the lowest, which is not due to
172 standard deviation being independent of C_G. Instead, the standard deviation increases
173 with C_G while the mean decreases with C_G **[SI Fig. 1].**

174 To better understand the potential role of heterotypic adhesion in determining
175 the speed of exit, we focused on the trajectories of the migrating cells at different values
176 of C_G. We ran our simulations for a maximum duration of 10,000 Monte Carlo steps (44),
177 and the cells which had not exited by then were considered to have failed to exit. In
178 **Figure 3c**, the trajectories from ~1000 independent iterations are shown for $C_G = 4.89$,
179 $C_E = 10.0$ and $\lambda_M = 7000$. While there are numerous instances of the migrating cell
180 failing at early stages of the transepithelial migration, we see many instances of germ

181 cells stuck to the outer edge of the epithelial barrier and failing to complete midgut exit.
182 We considered all the successful trajectories for $C_E = 10$ and $\lambda_M = 7000$ and normalized
183 the time for each trajectory, such that $\tau = 0$ and $\tau = 1$ mark the start and end of the
184 transepithelial migration respectively. The time-normalized mean trajectories are shown
185 in **Figure 3d**, colored according to their values of C_G. We observed that germ cells with
186 lower E-cadherin concentrations spent much of their time getting to the middle of the
187 epithelial barrier, while the second half of the journey, culminating in complete exit
188 from the midgut, was quite rapid. The fraction of total time spent in getting to the
189 middle dropped with increasing germ cell–epithelial cell adhesion, with speed through
190 the barrier becoming constant for high values of C_G (~7.0). To highlight the difference in
191 the fraction of total travel time spent at different halves of the epithelial barrier, we
192 show the fraction of time spent to cover the second half of the epithelial barrier (referred
193 to as τ_2) in **Figure 3d′**. τ_2 showed a nonlinear increase with C_G approaching 0.5 at lager
194 values of C_G. The probability of success in exiting the epithelial barrier had an inverse
195 non-linear relation to time to exit τ_e regardless of the C_E, C_G and λ_M, as evident from the
196 scatter plot in **Figure 3e**.

197

198 *III. Overexpression of E-cadherin in germ cells leads to faster exit through*
199 *the midgut*

200 The results of our model suggested that increasing E-cadherin levels in germ cells
201 would enable them to complete the most time-consuming part of their journey, namely
202 traversing from the middle of the midgut lumen through the luminal epithelial surface,
203 more rapidly, thus resulting in a faster net transepithelial migration time. To test this
204 prediction *in vivo*, we employed the UAS-GAL4 system (45). Maternally deposited E-
205 cadherin serves as the primary source of E-cadherin for all early embryonic cells,
206 including both germ cells and somatic cells (28, 30, 46). Notably, even during
207 transepithelial migration (~3 hours after egg laying), germ cell E-cadherin remains
208 predominantly of maternal origin, making RNAi-mediated knockdown in germ cells
209 impractical without destroying embryonic integrity (28, 30, 46).

210 Given these constraints, to assess the effects of E-cadherin overexpression on
211 transepithelial migration, we analyzed germ cell progression in embryos of four
212 different maternal genotypes, collected within 30 minutes from synchronously
213 ovipositing mothers and aged for five hours, as follows: (I) **WT**: Outcrossed wild-type
214 control, expressing endogenous levels of E-cadherin in all cells [*nos-Gal4/+*]; (II) **Pan-**
215 **Ecad-OE-A**: with ubiquitous E-cadherin overexpression in all cells [*nos>Ecad*]; (III) **Pan-**
216 **Ecad-OE-B**: with ubiquitous GFP-tagged E-cadherin overexpression in all cells
217 [*nos>Ecad-GFP*]; and (IV) **GC-Ecad-OE**: with germ cell-targeted overexpression of
218 mClover2-tagged E-cadherin [*nos> Ecad-mClover2-nosTCE-pgc 3'UTR*]. The position of
219 germ cells relative to the midgut lumen boundary in representative embryos from each
220 group is shown in **Figure 4a–a'''**. Quantitative analysis revealed that germ cells in all
221 overexpression lines (II–IV) were located farther from the lumen center compared to
222 controls (I) [**Fig. 4b**]. Furthermore, both the mean germ cell distance from the lumen
223 center [**Fig. 4c**] and the fraction of germ cells that had exited the midgut [f_{exit} in **Fig. 4d**]
224 were higher in overexpression groups, with the most pronounced effect in the germ
225 cell-targeted overexpression line (IV).

226 These results suggest that higher levels of E-cadherin in germ cells accelerates
227 transepithelial migration, consistent with our theoretical model. We favor the
228 interpretation that the germ cell E-cadherin expression corresponds to the gray region
229 in **Figure 4e**. Under this interpretation, loss of function *shg* mutants like shg^{A9-49} (30)
230 would drive the embryo toward the red region shown in **Figure 4e**, associated with
231 longer τ_e, while *shg* overexpression would drive it towards the green region in **Figure**
232 **4e** associated with faster germ cell exit.

233 Our model predicted that elevated epithelial E-cadherin would hinder migration
234 by increasing resistance to germ cell exit. Although our experiments did not test this
235 prediction directly, germ cells in our experiments overexpressing E-cadherin in both
236 somatic and germ cells showed reduced germ cell exit times. This apparent discrepancy
237 can be explained by the hypothesis that wild-type E-cadherin levels in somatic
238 epithelial cells are already near saturation. Under this interpretation, finite adhesion

239 junction availability and membrane transport limitations would prevent additional E-
240 cadherin from forming new junctions at high concentrations (47–50). Thus, in embryos
241 with E-cadherin overexpression in both germ cells and somatic cells, like the ones we
242 examined herein (**Fig. 4,** groups II and III), we hypothesize that E-cadherin levels higher
243 than wild type levels would have a stronger effect on germ cells than on epithelial cells,
244 effectively mimicking germ cell-specific overexpression.
245

246 ## Discussion

247 Our work sheds light on the potential role of heterotypic E-cadherin adhesion during
248 the transepithelial migration of germ cells through the midgut. The predictions of our *in*
249 *silico* model could in principle apply to any heterotypic adhesive migration process, as
250 we incorporated only a few features specific to germ cell transepithelial migration. Our
251 results suggest a non-monotonic dependence of migration efficiency on the heterotypic
252 adhesion between the migrating cell and the substrate cells [**Fig. 4d**]. We posit that
253 traction is essential for cell migration, and that transmembrane proteins like integrins
254 facilitate traction by anchoring cells to the extracellular matrix, thereby enabling
255 forward movement (51). Additionally, cadherin-like molecules mediate homotypic
256 adhesion, allowing cells of the same type to form cohesive tissues such as epithelia (46,
257 52). These molecules also participate in heterotypic adhesion when migrating cells
258 interact with others expressing cadherins (53–55). A notable example is the
259 transendothelial migration of melanoma cells, where heterotypic adhesion is clearly
260 observed (53). More broadly, diapedesis - the process by which cells breach endothelial
261 barriers - relies on heterotypic interactions between transmembrane adhesion proteins
262 (54, 55). The prevalence of heterotypic adhesion during transepithelial migration
263 suggests that our work may have broader implications beyond the specific context of
264 *Drosophila* primordial germ cell migration.

265 Many conserved features of cell migration are applicable well beyond a specific
266 biological context. In a migrating cell, actin filaments polymerize at the leading edge

267 and undergo retrograde flow, functioning much like the rotation of wheels in a car (56–
268 58). However, the forward motion of a cell depends on its physical coupling to the
269 substrate, just as the tires of a car grip the road to provide traction (56, 57, 59). This
270 mechanism is described by the *molecular clutch model* of cell motility (60). Adhesion
271 molecules such as integrins and cadherins allow cells to bind to surfaces or to other
272 cells, engaging the molecular clutch (60, 61). Integrin-mediated traction is typically used
273 when cells migrate over an extracellular matrix, whereas cadherins facilitate cell-on-cell
274 migration, as seen in the case of border cell migration (36, 61), and in the transepithelial
275 migration case that we consider here.

276 Our *in silico* model predicts that an intermediate adhesion strength between
277 migrating cells and substrate cells optimizes transmigration. Our finding aligns with
278 previous observations on *D. melanogaster* border cell migration in the egg chamber (36,
279 62). In the case of border cell migration, a cluster of six to eight border cells, enclosing a
280 pair of non-motile polar cells, migrates through a "substrate" formed by nurse cells (62).
281 Of these three cell types, polar cells express the highest levels of E-cadherin, which they
282 use to anchor to motile border cells, which have the second highest E-cadherin levels
283 (36). Meanwhile, border cells form transient junctions with nurse cell E-cadherin (which
284 is at the lowest levels of the three cell types in the system), pulling on nurse cells as they
285 migrate (36). Notably, E-cadherin knockdown in nurse cells impedes migration more
286 severely than knockdown in border cells, whereas E-cadherin overexpression in nurse
287 cells slows migration (36). These observations further support the concept that
288 intermediate heterotypic adhesion is optimal for transmigration, specifically E-cadherin
289 enabling the engagement of a molecular clutch (61). Migration in the absence of
290 sufficient intercellular adhesion resembles climbing a slippery ladder—lacking the
291 traction needed for upward movement. Conversely, excessive adhesion is akin to
292 ascending a ladder coated in glue, where detachment becomes the limiting factor. Thus,
293 an optimal level of "stickiness" is crucial for efficient migration.

294 **Methods**

295 ***Fly stocks and maintenance***

296 Fly lines *w[1118]; P{w[+mC]=GAL4::VP16-nanos.UTR}CG6325[MVD1]* (abbreviated
297 herein as *nanos-gal4-VP16*; stock #4937), *w[1118]; P{w[+mC]=UASp-shg.GFP}5B* (#58445),
298 *y[1] w[*]; TI{TI}shg[GFP]* (#60584), and *w[*]; P{w[+mC]=UASp-shg.R}5* (#58494) were
299 obtained from the Bloomington Drosophila Stock Center (Indiana, U.S.A.). Fly lines *w;*
300 *nos-Lifeact-tdTomato-P2A-tdKatushka2-CAAX (Lifeact-tdTomato* landing site VK00027;
301 abbreviated herein as *nos-LifeAct-tdTomato*) and *w; UASp-DE-cadherin-mClover2-nosTCE-*
302 *pgc 3'UTR* (landing site attP2) *(Lin et al., 2022)* were a gift from Ruth Lehmann
303 (Whitehead Institute, USA). All flies and crosses were maintained on standard fly
304 medium (0.8% agar, 2.75% yeast, 5.2% cornmeal, 11% dextrose) in an incubator at 25˚C,
305 65% RH and 12H:12H light-dark cycle.

306

307 ***Fly crosses and embryo staging***

308 To generate embryonic over-expression, UASp (over-expression) or Oregon R (wild
309 type control) lines were crossed to *nanos-gal4-VP16* and heterozygous F1 virgin females
310 were collected. 40-50 F1 virgin females were then crossed with 8-10 Oregon R males and
311 transferred into an egg collection cage with a 5mm apple juice agar plate as base (63). In
312 the case of *nos-LifeAct-tdTomato* flies, an approximate 1:1 ratio of homozygous males and
313 females were transferred into an identical cage setup. Egg laying was allowed to
314 proceed in 30-minute windows and embryos were aged for five hours after the
315 midpoint of the egg laying window. After collection, embryos were either fixed
316 (embryonic over-expression) or used for live imaging (*nos-LifeAct-tdTomato)*.

317

318 ***Live imaging***

319 Appropriately staged *nos-LifeAct-tdTomato* embryos were manually dechorionated with
320 forceps on double-sided scotch tape and attached to a standard 90 mm polystyrene Petri
321 dish using heptane glue. The dish was then filled with sterile distilled water and

322 mounted on a Zeiss LSM 980 multi-photon microscope. Using a 20x water immersion
323 objective, the total volume of the embryonic gut was imaged at a two-photon excitation
324 wavelength of 1000nm, every 5 or 10 minutes for the indicated period.

325

326 ***Fixation and immunostaining***

327 Appropriately staged embryos were collected on a mesh, rinsed with Milli-Q water, and
328 dechorionated using 70%(v/v) commercial bleach until most of the embryos had lost
329 the chorion (confirmed visually). Embryos were fixed in a 1:1 mix of heptane and 4%
330 paraformaldehyde in 1X phosphate buffered saline (1X PBS) at room temperature with
331 nutation for 20 minutes. After removing the aqueous layer, an equal volume of 100%
332 methanol was added, and embryos were devitellinized by vigorous manual shaking for
333 2–3 minutes. Fixed embryos were stored in 100% methanol at –20 °C.

334 For staining, embryos were rehydrated in 1X PBS, then washed, permeabilized
335 and blocked twice for 15 minutes in PBTB (1X PBS, 0.2% Triton X-100, 1 mg/mL bovine
336 serum albumin (Sigma-Aldrich, A9418). Embryos were then incubated with primary
337 antibodies diluted in PBTB overnight at 4 °C. The next day, embryos were washed (4 ×
338 15 min, PBTB) and incubated overnight at 4 °C with fluorophore-conjugated secondary
339 antibodies and DAPI diluted in PBTB containing 4% normal goat serum (Jackson
340 Immunoresearch, 005-000-121). On the third day, embryos were washed (4 × 15 min in
341 1X PBS) and mounted in Vectashield (Vector laboratories, H1000) for imaging.

342 Primary antibodies used were chicken anti-Vasa (1:800) (Repouliou et al., 2025)
343 and mouse anti-GFP conjugated to AlexaFluor 488 (1:1000; (Invitrogen, A-21311).
344 Secondary antibody used was goat anti-chicken (1:200) conjugated to AlexaFluor 568
345 (Invitrogen, A-11041). DNA was stained with DAPI (Sigma-Aldrich, D9542) at 1:2000
346 dilution of a 10 mg/mL stock.

347

348 ***In silico model of transepithelial migration***

349 A cross-sectional slice of the epithelial midgut was modelled as a two-dimensional ring
350 formed by 20 epithelial cells. The epithelial ring is embedded in a radial chemical field
351 representing the spatial concentration of the chemoattractant. The magnitude of the
352 chemical concentration increases linearly with the radius, and the minimum coincides
353 with the center of the epithelial ring. At t=0, the germ cell begins slightly off-center,
354 with its initial angle randomly chosen between 0 and 360 degrees, and then migrates
355 outward toward regions of higher chemoattractant concentration.

356 Our two-dimensional model of the epithelial ring and the germ cells was
357 formulated in the Cellular Potts Model (CPM) framework (37–39). The cells in a CPM
358 are represented as a contiguous collection of pixels. Pairwise interactions between
359 pixels at the cell boundaries have an associated energy cost, J. Given two pixels a and b,
360 we use the value of $J_{a,b}$ to reflect the adhesion energy of the cells to which the two
361 interacting boundary pixels belong. Our model assumes that adhesion energy increases
362 with the number of adherens junctions formed, and that the number of adherens
363 junctions is in turn a function of the E-cadherin concentration. The maximum possible
364 number of junctions between two cells is thus determined by the surface E-cadherin
365 concentration of the cell that has fewer such molecules. As a result of our assumptions,
366 if $\sigma(a)$, $\sigma(b)$ are the indices of the cells to which pixels a and b belong, and $C(\sigma(a))$ and
367 $C(\sigma(b))$ are the E-cadherin concentrations of the two cells, then the interaction energy
368 term is $J_{a,b} = min(C(\sigma(a)), C(\sigma(b)))$. In our work, we have assumed that all epithelial
369 cells have E-cadherin concentration equal to C_E, and that all germ cells have E-cadherin
370 concentration equal to C_G. The energy function of the system of pixels is given by the
371 following equation:

372 $$E = -\sum_{a,b} min(C(\sigma(a)), C(\sigma(b))) - \sum_{\sigma} \lambda_A (A_\sigma - A_0)^2 - \sum_{\sigma} \lambda_L (L_\sigma - L_0)^2$$

373 The λ_A and λ_L terms determine the magnitude of the energy cost required for a cell area
374 and perimeter to deviate from the steady state values A_0 and L_0 respectively. The
375 system is simulated using the metropolis algorithm (44), where the probability of a pixel
376 flip is related to the change in the magnitude of the energy of the system as a result of
377 that specific pixel flip. Under appropriate energy conditions, pixels at the boundary

may flip to the cell state of one of their neighbors that has a different cell state. At each iteration of the simulation algorithm, one such potential pixel flip is considered, and the pixel is flipped if the resulting system has lower energy than the current state. If the pixel flip would not reduce the energy of the system, the pixel flips with probability $p_{flip} = exp(-\Delta E/T)$, where ΔE is the change in energy due to the pixel flip and T is the temperature. The temperature term T represents the extent of stochasticity (noise) in the pixel dynamics, with higher T increasing the probability of pixel flips that increase the energy of the system. Chemotaxis is implemented within the CPM framework by biasing pixel flips that aid cell movement in the direction of the gradient of chemoattractant. In the presence of the attractant whose value at any pixel in 2D space is $M_{a,b}$, the change in energy due to a pixel flip, where a pixel at (a, b) is copying the state of a pixel at (a', b') becomes $\Delta E' = \Delta E - \lambda_C\left(M_{a',b'} - M_{a,b}\right)$ (39). This additional term favors the pixel flip when the chemical field value at (a', b') is higher than (a, b). To prevent the epithelial ring from collapsing and forming a cell aggregate without a lumen, we model the lumen as one large cell with a volume constraint. In addition, we mechanically couple the epithelial cells by connecting the centroids of the adjacent cells with springs using the FocalPointPlasticity plugin of CompuCell3D (64). The key parameters that we explored in our work are C_G, C_E and λ_M. The CompuCell3D implementation of our model can be found at https://github.com/boyonpointe/GermCellTransepithelialMigration with commit ID 7ce2534.

Acknowledgements

We thank members of the Extavour Lab for helpful discussions, and Ruth Lehmann for sharing fly lines.

Data Availability

Scripts for Compucell3D simulations and image analysis are available at https://github.com/boyonpointe/GermCellTransepithelialMigration with commit ID 7ce2534.

Author Contributions

CK conceived of the study, designed and performed all computational experiments, performed data analysis and interpretation, and wrote the first draft of the manuscript. SG conceived of the study, designed and performed wet lab experiments, and reviewed and edited the manuscript. CGE obtained funding for the study, supervised its execution, and reviewed and edited the manuscript.

Funding

This study was supported by a postdoctoral fellowship to CK through the NSF-Simons Center for Mathematical and Statistical Analysis of Biology at Harvard (award number DMS-1764269), the Harvard Quantitative Biology Initiative, and by funds from Harvard University and the Howard Hughes Medical Institute (HHMI). CGE is an HHMI Investigator.

Conflicts of Interest

The authors declare no conflicts of interest.

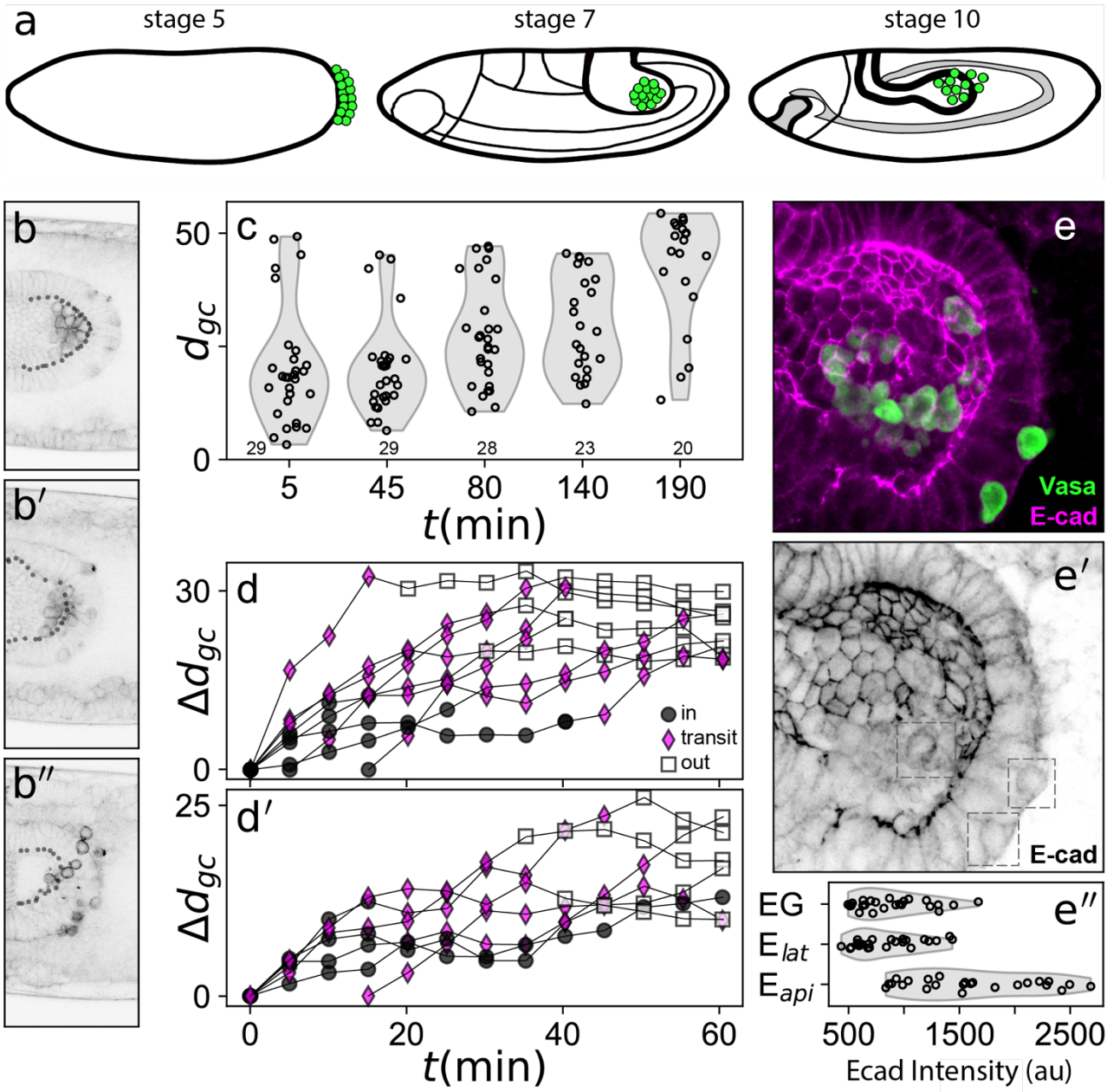

Figure 1: Germ cells exit the midgut individually at comparable speeds. (a-a′′) Schematic of *D. melanogaster* embryonic germ line development. The primordial germ cells are formed at the posterior tip at stage 5. Following gastrulation, they are contained in the midgut at stage 7, and eventually exit the midgut through transepithelial migration at stage 10. **(b-b′′)** Three snapshots from live imaging of the TEM process as the germ cells make their way through the midgut. **(c)** The distribution of the distances of the germ cells from center of the midgut lumen at five different time points are shown. Small numbers under plots indicate sample sizes (number of cells). **(d- d′′)** Movement of germ cells in time measured with respect to their initial (t = 0) position for two different live imaged embryos. Black circles: positions within lumen; magenta rhomboids: positions within the midgut epithelium; white squares: positions outside the midgut. **(e)** Higher magnification of the midgut during germ cell transepithelial migration. Magenta: E-cadherin; green: germ cell-specific protein Vasa. **(e′)** Germ cells express E-cadherin during the transepithelial migration (boxes). **(e′′)** The relative intensity (au: arbitrary units) of the E-cadherin fluorescent signal at the epithelial cell – germ cell junction (EG), lateral epithelial – epithelial junction (E_{lat}) and apical epithelial – epithelial junctions (E_{api}). n = 24 junctions for all categories.

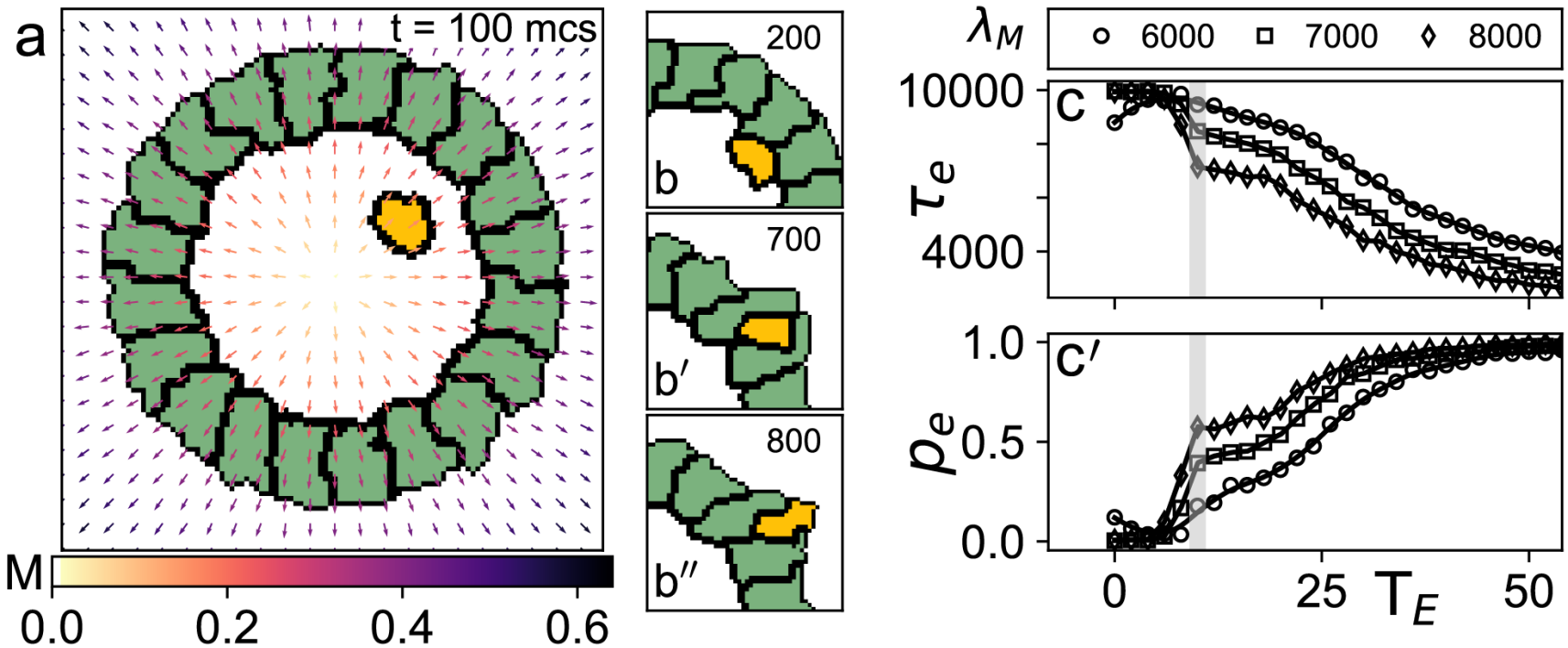

Figure 2: Greater epithelial junctional remodeling aids germ cell transmigration. (**a)** Snapshot of Cellular Potts Model simulation of a germ cell (yellow) exiting the two-dimensional epithelial ring (green). Pixels at the boundary of the cells are shown in black. Colored arrows point in the direction of chemoattractant gradient; colors represent the concentration of the chemoattractant. **(b-b′′)** Snapshots of the germ cell (b) before entering the epithelial barrier, (b′) while inside the barrier and (b′′) just before exiting the barrier. Numbers at top right indicate the time in units of Monte Carlo steps (mcs). **(c)** Average time taken (τ_e) for the germ cell to exit the midgut decreases with increase in interepithelial dynamics (T_E). **(c′)** Probability of successfully exiting (p_e) increases with T_E. Trends in c and c′ are independent of the strength of the chemoattractant (λ_M). The shaded silver line corresponds to $T_E = 10$, the value at which al simulations described herein are carried out, unless specified otherwise. Simulation parameters: $\lambda_M = 7000, C_E = 10, C_G = 5, T = 10$.

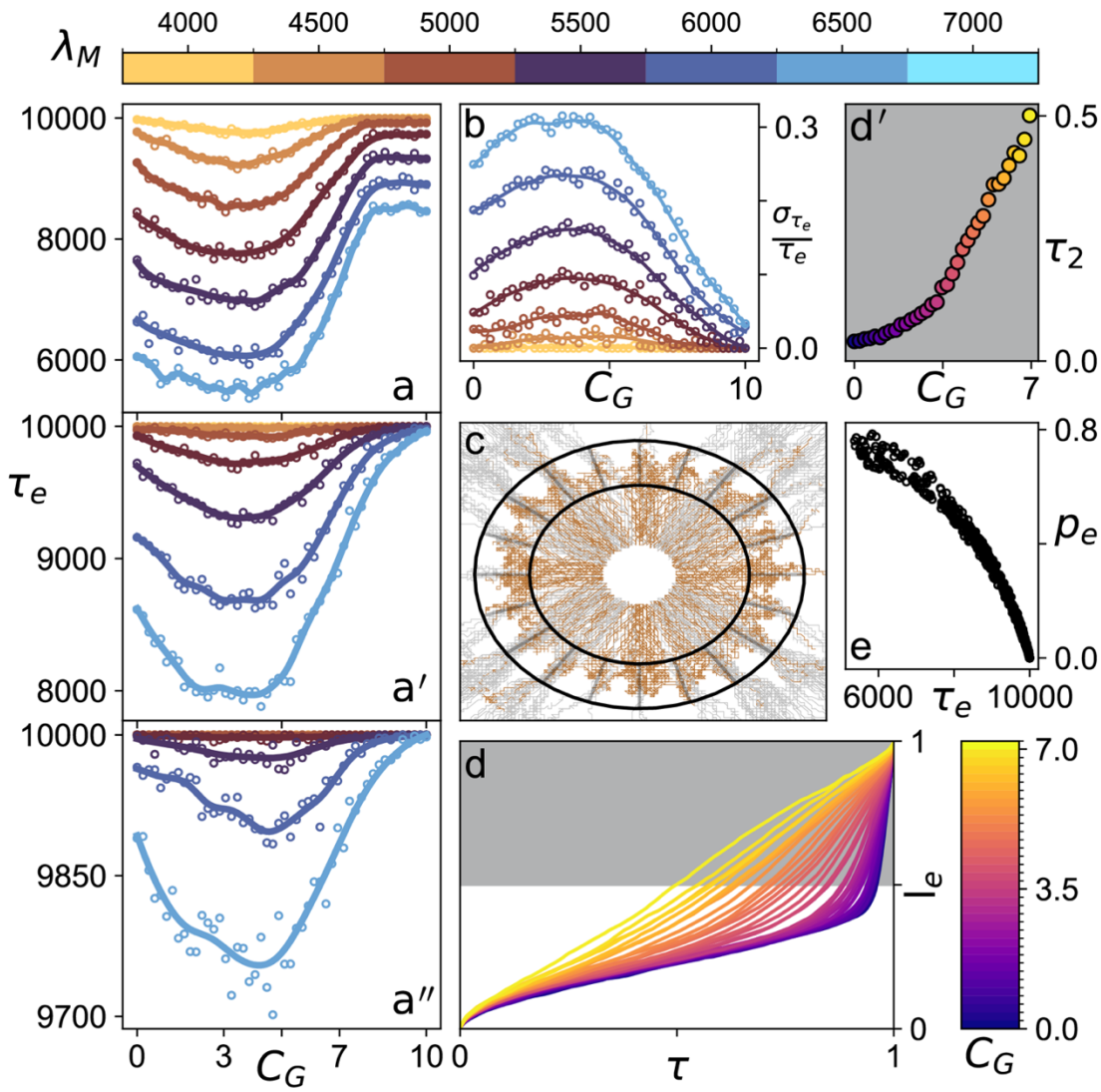

Figure 3: Time to exit the epithelial barrier has a non-monotonic dependence on germ cell E-cadherin concentration. (a-a′′) The time a simulated germ cell takes to exit the 2D midgut epithelial barrier as a function of germ cell E-cadherin concentration (C_G). (a), (a′) and (a′′) represent increasing epithelial cell E-cadherin concentrations ($C_E = 8$, $C_E = 10$, $C_E = 12$ respectively), offering increasing resistance to the germ cell transepithelial migration. The curves in each of the three panels are colored according to the strength of the chemical field (λ_M). Regardless of the value of C_E, for strong enough values of λ_M the time to exit shows a minimum that is independent of the λ_M value. **(b)** The coefficient of variation in time to exit as a function of C_G for the case of $C_E = 10$. **(c)** Trajectories of germ cells for a typical parameter set obtained from 1000 independent stochastic simulations. Silver: successful TEM; brown: germ cell exit failure; black lines: mean position of the epithelial cells forming the 2D barrier. **(d)** Mean distance covered by the germ cell within the barrier (l_e) as a function of time . The time τ is normalized by the total time of travel, where 0 represents time of entry into the barrier and 1 represents time of exit. When the germ cell E-cadherin concentration is low, the germ cell covers much of the distance in a very short interval of time at the end of the journey. Higher germ cell E-cadherin levels lead to the germ cell migrating at roughly uniform speed throughout the journey. **(d′)** The time taken to cover the second half of the journey τ_2 as a function of germ cell E-cadherin concentration. **(e)** The relationship between τ_{exit} and p_{exit} is shown using data aggregated by simulating the model over various values of λ_M, C_G and C_E. τ_{exit} decreases monotonically with p_{exit}, implying that the shorter the time to exit, the higher the chances of exiting.

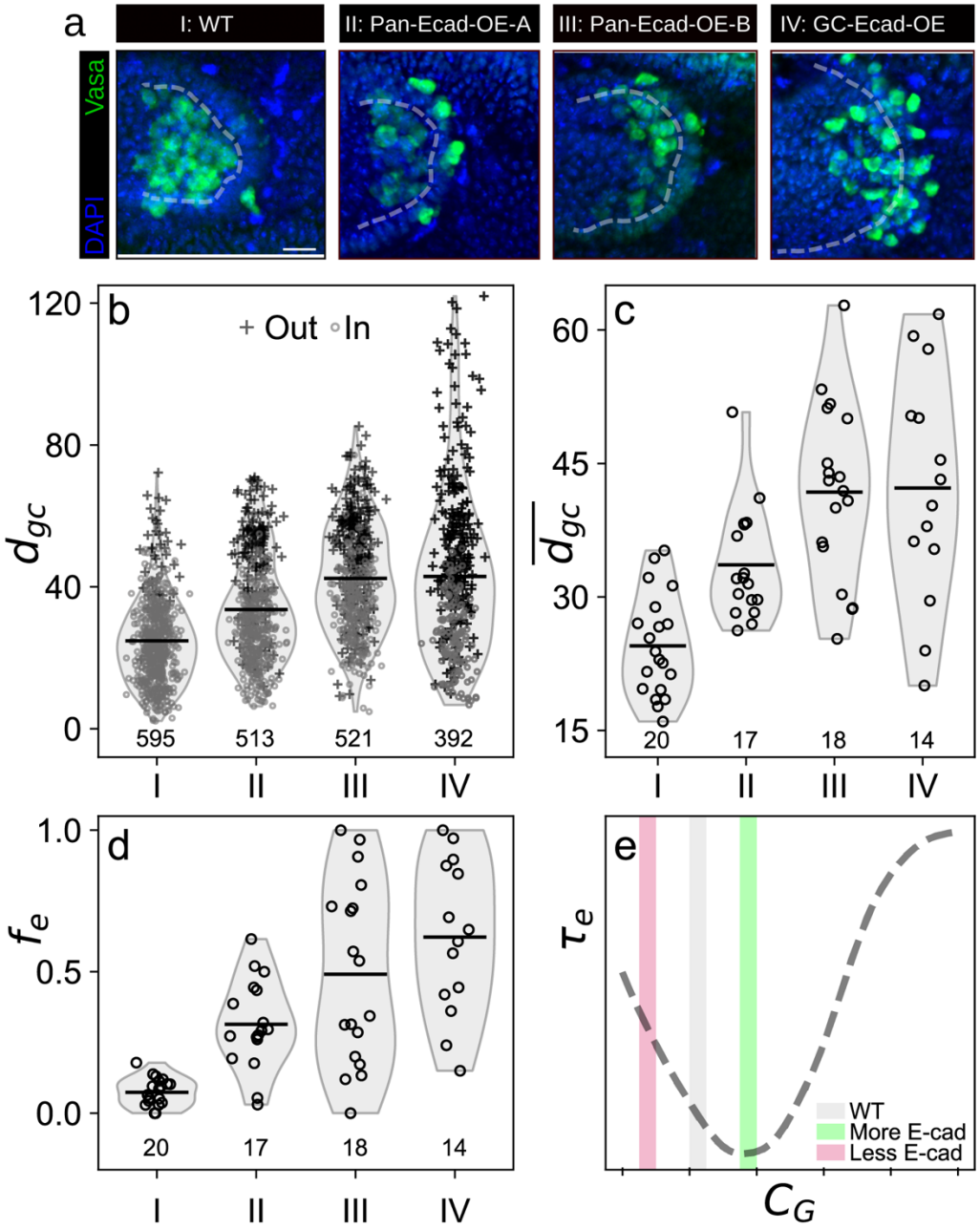

Figure 4: Higher germ cell E-cadherin promotes quicker midgut exit *in vivo*. (a) (L-R) Representative micrographs showing the extent of transepithelial migration in the four experimental groups. I corresponds to the control, II and III represent lines where E-cadherin is overexpressed in all cells and IV corresponds to embryos where E-cadherin overexpression is targeted to the germ cells. **(b)** The distribution of distances of germ cells from the center of the lumen for the four experimental groups. Grey and black symbols represent cells inside and outside the gut respectively. The distances of the germ cells from the lumen are largest in the condition with increased germ cell-targeted E-cadherin overexpression (IV). Small numbers under plots indicate sample sizes (number of germ cells). **(c)** Mean distance of the germ cells from the center of the lumen in each embryo for the four experimental groups. Small numbers under plots indicate sample sizes (number of embryos). **(d)** Fractions of germ cells per embryo that have exited the midgut by 5.25 hours after egg laying in the four experimental groups. Small numbers under plots indicate sample sizes (number of embryos). **(e)** We hypothesize that the WT embryos (group I) have C_G in the pink shaded region, and that germ cell-targeted E-cadherin expression pushes the system towards the green shaded region, leading to shortening of τ_e.

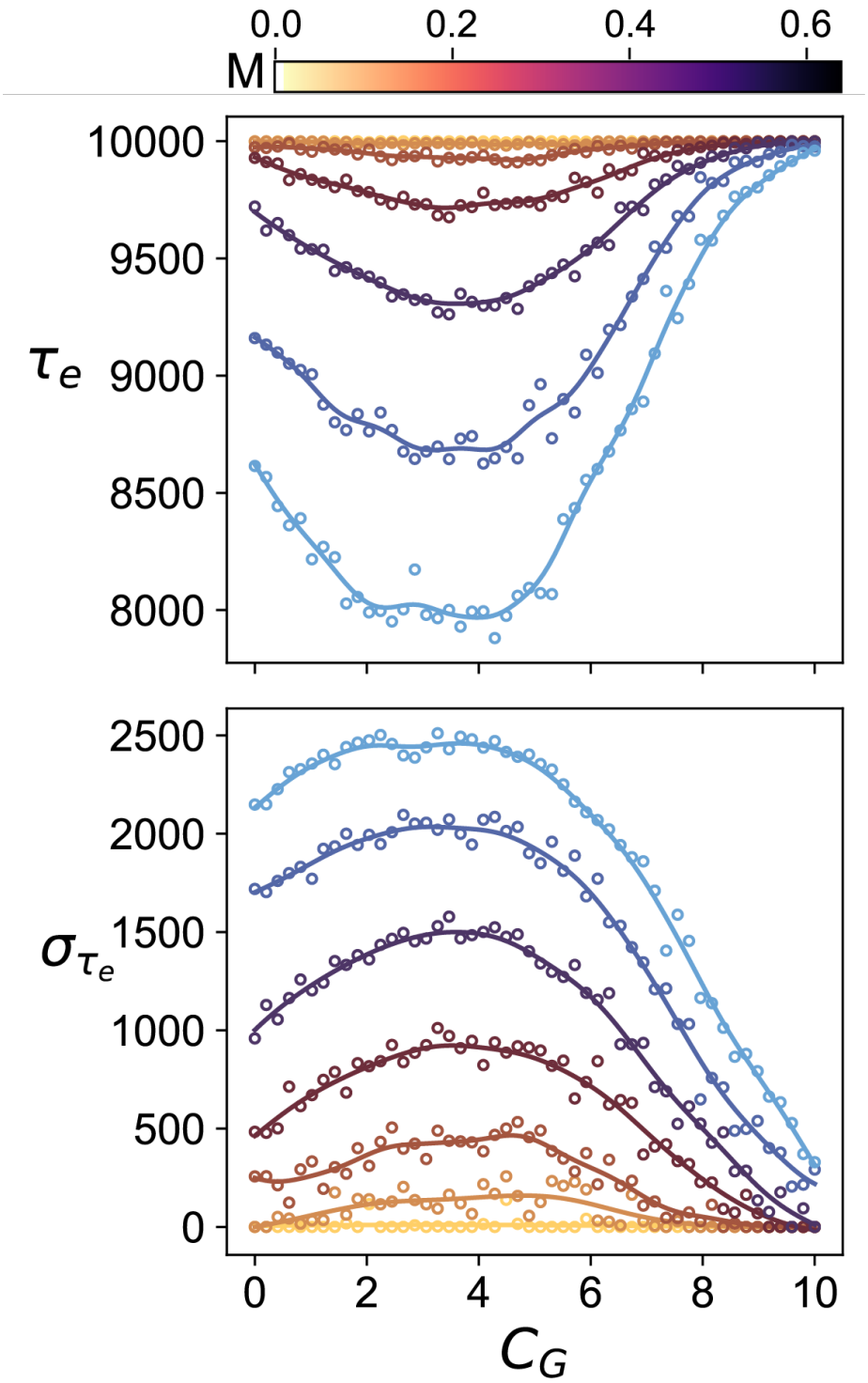

SI Figure 1: **The mean and the variance of τ_e exhibit converse trends.** The figure shows the mean τ_e (top) and standard deviation μ_{τ_e} (bottom) as a function of germ cell E-cadherin concentration C_G for the case when $C_E = 10$. The peak in the standard deviation as a function of C_G coincides with the minima in the case of time to exit. The differently colored curves correspond to different strengths of the chemoattractant pull λ_M .

SI Video Legends

SI Video 1: Transepithelial migration of germ cells. Dorsal cross-sectional view of the gut during TEM in a *nos-LifeAct-tdTomato* embryo. Maximum intensity projection of 15 planes spaced at 2 μm. Scale bar is 20 μm.

SI Video 2: Transepithelial migration of germ cells: higher magnification 1. Dorsal cross-sectional view of the gut during TEM in a *nos-LifeAct-tdTomato* embryo. Maximum intensity projection of 20 planes spaced at 2 μm. Scale bar is 20 μm.

SI Video 3: Transepithelial migration of germ cells: higher magnification 2. Lateral cross-sectional view of the gut during TEM in a *nos-LifeAct-tdTomato* embryo. Maximum intensity projection of 20 planes spaced at 2 μm. Scale bar is 20 μm.

SI Video 4: CompuCell3D simulation of a germ cell successfully exiting the midgut. The video shows an instance of a germ cell successfully exiting the epithelial ring in our *in silico* model simulated in CompuCell3D. The parameter values used here are $\lambda_M = 4000, C_G = 5.0, C_E = 10.0$.

SI Video 5: CompuCell3D simulation of a germ cell failing to exit the midgut. The video shows an instance of a germ cell failing to exit the epithelial ring in our *in silico* model simulated in CompuCell3D. The parameter values used here are $\lambda_M = 4000, C_G = 1.0, C_E = 10.0$.

References

1. A. Aman, T. Piotrowski, Cell migration during morphogenesis. *Dev. Biol.* **341**, 20–33 (2010).

2. E. Scarpa, R. Mayor, Collective cell migration in development. *J. Cell Biol.* **212**, 143–155 (2016).

3. D. Dormann, C. J. Weijer, Chemotactic cell movement during development. *Curr. Opin. Genet. Dev.* **13**, 358–364 (2003).

4. P. Roca-Cusachs, R. Sunyer, X. Trepat, Mechanical guidance of cell migration: lessons from chemotaxis. *Curr. Opin. Cell Biol.* **25**, 543–549 (2013).

5. E. T. Roussos, J. S. Condeelis, A. Patsialou, Chemotaxis in cancer. *Nat. Rev. Cancer* **11**, 573–587 (2011).

6. S. SenGupta, C. A. Parent, J. E. Bear, The principles of directed cell migration. *Nat. Rev. Mol. Cell Biol.* **22**, 529–547 (2021).

7. M. Bezanilla, A. S. Gladfelter, D. R. Kovar, W.-L. Lee, Cytoskeletal dynamics: A view from the membrane. *J. Cell Biol.* **209**, 329–337 (2015).

8. K. Rottner, T. E. B. Stradal, Actin dynamics and turnover in cell motility. *Curr. Opin. Cell Biol.* **23**, 569–578 (2011).

9. S. Seetharaman, S. Etienne-Manneville, Cytoskeletal Crosstalk in Cell Migration. *Trends Cell Biol.* **30**, 720–735 (2020).

10. S. F. Gilbert, S. F. Gilbert, *Developmental Biology*, 6th Ed. (Sinauer Associates, 2000).

11. P. Friedl, D. Gilmour, Collective cell migration in morphogenesis, regeneration and cancer. *Nat. Rev. Mol. Cell Biol.* **10**, 445–457 (2009).

12. W. T. Boyce, M. B. Sokolowski, G. E. Robinson, Genes and environments, development and time. *Proc. Natl. Acad. Sci.* **117**, 23235–23241 (2020).

13. M. Ebisuya, J. Briscoe, What does time mean in development? *Development* **145**, dev164368 (2018).

14. A. Kicheva, M. Cohen, J. Briscoe, Developmental Pattern Formation: Insights from Physics and Biology. *Science* **338**, 210–212 (2012).

15. J. Negrete, A. C. Oates, Towards a physical understanding of developmental patterning. *Nat. Rev. Genet.* **22**, 518–531 (2021).

16. C. M. Franz, G. E. Jones, A. J. Ridley, Cell Migration in Development and Disease. *Dev. Cell* **2**, 153–158 (2002).

17. C. J. Weijer, Collective cell migration in development. *J. Cell Sci.* **122**, 3215–3223 (2009).

18. A. F. Huettner, The origin of the germ cells in Drosophila melanogaster. *J. Morphol.* **37**, 385–423 (1923).

19. M. Rabinowitz, Studies on the cytology and early embryology of the egg of Drosophila melanogaster. *J. Morphol.* **69**, 1–49 (1941).

20. M. K. Jaglarz, K. R. Howard, The active migration of Drosophila primordial germ cells. *Development* **121**, 3495–3503 (1995).

21. A. C. Santos, R. Lehmann, Germ Cell Specification and Migration in Drosophila and beyond. *Curr. Biol.* **14**, R578–R589 (2004).

22. K. Hanyu-Nakamura, S. Kobayashi, A. Nakamura, Germ cell-autonomous Wunen2 is required for germline development in Drosophila embryos. *Development* **131**, 4545–4553 (2004).

23. A. D. Renault, Y. J. Sigal, A. J. Morris, R. Lehmann, Soma-Germ Line Competition for Lipid Phosphate Uptake Regulates Germ Cell Migration and Survival. *Science* **305**, 1963–1966 (2004).

24. H. Sano, A. D. Renault, R. Lehmann, Control of lateral migration and germ cell elimination by the Drosophila melanogaster lipid phosphate phosphatases Wunen and Wunen 2. *J. Cell Biol.* **171**, 675–683 (2005).

25. M. Slaidina, R. Lehmann, Quantitative Differences in a Single Maternal Factor Determine Survival Probabilities among Drosophila Germ Cells. *Curr. Biol.* **27**, 291–297 (2017).

26. R. Warrior, Primordial Germ Cell Migration and the Assembly of the Drosophila Embryonic Gonad. *Dev Biol* **166**, 180–194 (1994).

27. H. Oda, T. Uemura, Y. Harada, Y. Iwai, M. Takeichi, A *Drosophila* Homolog of Cadherin Associated with Armadillo and Essential for Embryonic Cell-Cell Adhesion. *Dev. Biol.* **165**, 716–726 (1994).

28. U. Tepass, *et al.*, shotgun encodes Drosophila E-cadherin and is preferentially required during cell rearrangement in the neurectoderm and other morphogenetically active epithelia. *Genes Dev.* **10**, 672–685 (1996).

29. M. DeGennaro, *et al.*, Peroxiredoxin Stabilization of DE-Cadherin Promotes Primordial Germ Cell Adhesion. *Dev. Cell* **20**, 233–243 (2011).

30. P. S. Kunwar, *et al.*, Tre1 GPCR initiates germ cell transepithelial migration by regulating Drosophila melanogaster E-cadherin. *J. Cell Biol.* **183**, 157–168 (2008).

31. P. S. Kunwar, M. Starz-Gaiano, R. J. Bainton, U. Heberlein, R. Lehmann, Tre1, a G Protein-Coupled Receptor, Directs Transepithelial Migration of Drosophila Germ Cells. *PLoS Biol.* **1**, e80 (2003).

32. J. A. Campos-Ortega, V. Hartenstein, *The Embryonic Development of Drosophila melanogaster* (Springer Science & Business Media, 2013).

33. D. Poulson, D. Waterhouse, Experimental Studies on Pole Cells and Midgut Differentiation in Diptera. *Aust. J. Biol. Sci.* **13**, 541–567 (1960).

34. J. R. K. Seifert, R. Lehmann, Drosophila primordial germ cell migration requires epithelial remodeling of the endoderm. *Development* **139**, 2101–2106 (2012).

35. G. Parés, S. Ricardo, FGF control of E-cadherin targeting in the Drosophila midgut impacts on primordial germ cell motility. *J. Cell Sci.* **129**, 354–366 (2016).

36. D. Cai, *et al.*, Mechanical Feedback through E-Cadherin Promotes Direction Sensing during Collective Cell Migration. *Cell* **157**, 1146–1159 (2014).

37. J. A. Glazier, F. Graner, Simulation of the differential adhesion driven rearrangement of biological cells. *Phys. Rev. E* **47**, 2128–2154 (1993).

38. F. Graner, J. A. Glazier, Simulation of biological cell sorting using a two-dimensional extended Potts model. *Phys. Rev. Lett.* **69**, 2013–2016 (1992).

39. P. Hogeweg, Evolving Mechanisms of Morphogenesis: on the Interplay between Differential Adhesion and Cell Differentiation. *J. Theor. Biol.* **203**, 317–333 (2000).

40. D. Sweeton, S. Parks, M. Costa, E. Wieschaus, Gastrulation in Drosophila: the formation of the ventral furrow and posterior midgut invaginations. *Development* **112**, 775–789 (1991).

41. B. Lin, J. Luo, R. Lehmann, An AMPK phosphoregulated RhoGEF feedback loop tunes cortical flow–driven amoeboid migration in vivo. *Sci. Adv.* **8**, eabo0323 (2022).

42. M. Akhmanova, *et al.*, Cell division in tissues enables macrophage infiltration. *Science* **376**, 394–396 (2022).

43. M. K. Jaglarz, K. R. Howard, Primordial germ cell migration in Drosophila melanogaster is controlled by somatic tissue. *Development* **120**, 83–89 (1994).

44. N. Metropolis, A. W. Rosenbluth, M. N. Rosenbluth, A. H. Teller, E. Teller, Equation of State Calculations by Fast Computing Machines. *J. Chem Phys.* **21**, 1087–1092 (1953).

45. A. H. Brand, N. Perrimon, Targeted gene expression as a means of altering cell fates and generating dominant phenotypes. *Development* **118**, 401–415 (1993).

46. T. J. C. Harris, U. Tepass, Adherens junctions: from molecules to morphogenesis. *Nat. Rev. Mol. Cell Biol.* **11**, 502–514 (2010).

47. S. Hong, R. B. Troyanovsky, S. M. Troyanovsky, Binding to F-actin guides cadherin cluster assembly, stability, and movement. *J. Cell Biol.* **201**, 131–143 (2013).

48. R. B. Troyanovsky, E. P. Sokolov, S. M. Troyanovsky, Endocytosis of Cadherin from Intracellular Junctions Is the Driving Force for Cadherin Adhesive Dimer Disassembly. *MBoC* **17**, 3484–3493 (2006).

49. B.-A. Truong Quang, M. Mani, O. Markova, T. Lecuit, P.-F. Lenne, Principles of E-Cadherin Supramolecular Organization In Vivo. *Curr. Biol.* **23**, 2197–2207 (2013).

50. Y. Wu, P. Kanchanawong, R. Zaidel-Bar, Actin-Delimited Adhesion-Independent Clustering of E-Cadherin Forms the Nanoscale Building Blocks of Adherens Junctions. *Dev. Cell* **32**, 139–154 (2015).

51. A. Huttenlocher, Cell polarization mechanisms during directed cell migration. *Nat. Cell Biol.* **7**, 336–337 (2005).

52. J. M. Halbleib, W. J. Nelson, Cadherins in development: cell adhesion, sorting, and tissue morphogenesis. *Genes Dev.* **20**, 3199–3214 (2006).

53. M. Sandig, E. B. Voura, V. I. Kalnins, C.-H. Siu, Role of cadherins in the transendothelial migration of melanoma cells in culture. *Cell Motil. Cytoskelet.* **38**, 351–364 (1997).

54. D. Vestweber, How leukocytes cross the vascular endothelium. *Nat. Rev. Immunol.* **15**, 692–704 (2015).

55. Y.-T. Yeh, *et al.*, Three-dimensional forces exerted by leukocytes and vascular endothelial cells dynamically facilitate diapedesis. *Proc. Natl. Acad. Sci.* **115**, 133–138 (2018).

56. C. E. Chan, D. J. Odde, Traction Dynamics of Filopodia on Compliant Substrates. *Science* **322**, 1687–1691 (2008).

57. P. Maiuri, *et al.*, Actin Flows Mediate a Universal Coupling between Cell Speed and Cell Persistence. *Cell* **161**, 374–386 (2015).

58. K. M. Yamada, M. Sixt, Mechanisms of 3D cell migration. *Nat. Rev. Mol. Cell Biol.* **20**, 738–752 (2019).

59. V. Swaminathan, C. M. Waterman, The molecular clutch model for mechanotransduction evolves. *Nat. Cell Biol.* **18**, 459–461 (2016).

60. L. B. Case, C. M. Waterman, Integration of actin dynamics and cell adhesion by a three-dimensional, mechanosensitive molecular clutch. *Nat. Cell Biol.* **17**, 955–963 (2015).

61. L. J. Barton, L. R. la Cruz, R. Lehmann, B. Lin, The journey of a generation: advances and promises in the study of primordial germ cell migration. *Development* **151**, dev201102 (2024).

62. D. J. Montell, P. Rorth, A. C. Spradling, slow border cells, a locus required for a developmentally regulated cell migration during oogenesis, encodes Drosophila CEBP. *Cell* **71**, 51–62 (1992).

63. W. F. Rothwell, W. Sullivan, Drosophila Embryo Collection. *Cold Spring Harb. Protoc.* **2007**, pdb.prot4825 (2007).

64. M. H. Swat, *et al.*, Multi-Scale Modeling of Tissues Using CompuCell3D. *Methods Cell Biol.* **110**, 325–366 (2012).